THE ASTROPHYSICAL JOURNAL, 392:485–491, 1992 June 20

HOPKINS ULTRAVIOLET TELESCOPE OBSERVATIONS OF THE FAR-ULTRAVIOLET SPECTRUM OF NGC 4151

G. A. KRISS,[1] A. F. DAVIDSEN,[1] WILLIAM P. BLAIR,[1] C. W. BOWERS,[1] W. V. DIXON,[1] S. T. DURRANCE,[1] P. D. FELDMAN,[1] H. C. FERGUSON,[2] R. C. HENRY,[1] R. A. KIMBLE,[3] J. W. KRUK,[1] KNOX S. LONG,[4] H. W. MOOS,[1] AND O. VANCURA[1]

Received 1991 November 11; accepted 1991 December 27

ABSTRACT

We observed the far-ultraviolet spectrum of the Seyfert galaxy NGC 4151 from 912 to 1860 Å with the Hopkins Ultraviolet Telescope during the flight of Astro-1 aboard the space shuttle *Columbia* in 1990 December. Broad emission lines with full-width at half-maximum of $\sim$8500 km s^{-1} dominate the spectrum. Numerous absorption features modify the continuum shape, particularly at wavelengths shortward of Lyα. The continuum turns over sharply below 1000 Å and disappears by 924 Å, well above the redshifted Lyman edge of NGC 4151 at 915 Å. The continuum flux and the intensity of broad C IV λ1549 are slightly above the historical mean values observed with the *International Ultraviolet Explorer*. Many of the spectral features in the 912–1150 Å range have never before been seen in a low-redshift activity galaxy, including emission from O VI $\lambda\lambda$1032, 1037 and He II λ1085, and absorption by C III λ977, N III λ991, O VI $\lambda\lambda$1032, 1037, and the hydrogen Lyman series. The broad emission lines all have similar profiles, and their relative intensities are consistent with previously calculated photoionization models. The absorption lines have intrinsic widths of $\sim$1000 km s^{-1} and are blueshifted relative to the systemic velocity of NGC 4151 by 200–1300 km s^{-1}. The observed equivalent widths of the C III absorption lines λ977 and λ1176 require absorbing material with a density in excess of $10^{9.5}$ cm^{-3}. The equivalent widths of these same lines, the Si IV doublet $\lambda\lambda$1393, 1402, and the hydrogen Lyman lines all favor a Doppler parameter $b \simeq 200$ km s^{-1} for the absorbing material. Absorption of the continuum by the converging higher order Lyman lines explains the sharp turnover of the continuum below 1000 Å. The blueshifts of the absorption lines, their large intrinsic widths, and the inferred high densities are all consistent with outflowing material originating in the broad-line region.

Subject headings: galaxies: individual (NGC 4151) — galaxies: nuclei — galaxies: Seyfert — ultraviolet: galaxies

1. INTRODUCTION

As the brightest and one of the nearest Seyfert 1 galaxies, NGC 4151 is a touchstone for understanding the structure and physical processes at work in active galactic nuclei. One of the original 12 galaxies cataloged by Seyfert (1943), NGC 4151 was classified as a Seyfert 1.5 by Osterbrock & Koski (1976) because of the prominent narrow forbidden lines in its spectrum in addition to the broad permitted lines characteristic of the Seyfert 1 class. The emission-line profiles are complex, and different lines have different profiles, indicating stratification of the line-emitting region (Ulrich et al. 1984; Clavel et al. 1987). The broad lines, their profiles, and the nonthermal continuum all vary with time. This variability has been used to unravel the structure of the broad line region through studies at ultraviolet (Ulrich et al. 1984; Clavel et al. 1987; Clavel et al. 1991) and optical (Antonucci & Cohen 1983; Maoz et al. 1991) wavelengths.

The strong absorption seen in the optical, ultraviolet, and X-ray spectra of NGC 4151 is unique among active galaxies. The X-ray spectrum NGC 4151 is absorbed at low energies by material with an inferred column density of $N_H = 10^{22}$ cm^{-2}. The absorption is incomplete, however, and $\sim$10% of the continuum appears to "leak" through the absorbing material (Holt et al. 1980). Ferland & Mushotzky (1982) identified the material that partially covers the ionizing source as the broad-line gas of NGC 4151, and argued that the widths and column densities inferred for the Balmer absorption lines (Anderson 1974) and many ultraviolet absorption lines (Penston et al. 1981) were consistent with this view. On the other hand, from an intensive study of the ultraviolet absorption lines and their variability, Bromage et al. (1985) concluded that the ultraviolet absorption lines must arise in several different locations within and just outside the broad-line region in material that is distinct from that emitting the broad lines.

The far-ultraviolet spectral region from Lyα at 1216 Å to the Lyman edge at 912 Å is rich in spectral diagnostics, containing the hydrogen Lyman lines as well as the resonance transitions of many metallic species. Because this spectral range has been largely inaccessible in nearby active galactic nuclei (AGNs), far-UV observations of the nearest and brightest AGNs form one of the prime scientific programs for the Hopkins Ultraviolet Telescope (HUT). To gain added insights into the nature of NGC 4151, we observed the far-ultraviolet spectrum of its active nucleus with HUT during the first flight of the Astro Observatory aboard the space shuttle *Columbia*.

2. OBSERVATIONS AND DATA REDUCTION

HUT comprises a 0.9 m primary mirror feeding a prime-focus, Rowland-circle spectrograph (Davidsen et al. 1992). The

[1] Center for Astrophysical Sciences, Department of Physics and Astronomy, The Johns Hopkins University, Baltimore, MD 21218.
[2] Institute of Astronomy, Cambridge University, The Observatories, Madingley Road, Cambridge CB3 0HA, England, UK.
[3] Laboratory for Astronomy and Solar Physics, Code 681, NASA/Goddard Space Flight Center, Greenbelt, MD 20771.
[4] Space Telescope Science Institute, 3701 San Martin Drive, Baltimore, MD 21218.

dispersed photons are imaged onto a photon-counting, microchannel-plate detector with a phosphor-screen/Reticon-diode-array readout. First-order spectra cover the spectra range 830–1860 Å with a sampling of 0.51 Å per pixel and a point-source resolution of ~3 Å. In practice, neutral hydrogen absorption by the interstellar medium of our own Galaxy limits the shortest observable wavelength to 912 Å for all but the nearest objects in our Galaxy.

We observed NGC 4151 with HUT for a total integration time of 2188 s on 1990 December 8. The observation began during orbital night. Approximately 400 s of terrestrial airglow and background data were obtained before NGC 4151 was placed in the entrance aperture as the field was verified on the acquisition TV camera. We accumulated 900 s of data on the target during orbital night before the shuttle crossed the terminator into the daylight portion of the orbit where the airglow is much stronger. After NGC 4151 was centered in the 18″ circular aperture, the pointing was very stable, with rms deviations of only 2″.1, as judged by the locations of guide stars in the HUT acquisition TV camera relative to reference fiducials; there were no excursions large enough to move the target out of the aperture.

The raw HUT data were transformed into IRAF[5] image files for reduction and analysis. The raw count rate data were corrected for pulse persistence in the phosphor readout. Detector background and grating-scattered geocoronal Lyα were determined from regions free of airglow below the 912 Å Lyman limit. We subtracted background and placed the spectrum on an absolute flux scale by dividing by the effective area curve developed from observations of the hot white dwarf G191-B2B (Davidsen et al. 1992).

The HUT wavelength scale is linear to high accuracy. Analysis of airglow line positions throughout the mission verifies that the preflight calibration is stable on-orbit to ±1 Å. Placement of a point source target in the entrance aperture can introduce zero-point shifts, however. The wavelength scale for the NGC 4151 observation was verified to be accurate to better than 0.3 Å by comparing the positions of narrow emission and absorption features in the spectrum longward of 1200 Å to those determined from high-resolution spectra obtained with the *International Ultraviolet Explorer* (*IUE*) (Bromage et al. 1985).

To achieve the highest possible signal-to-noise ratio (S/N) in the final spectrum, the orbital night data were reduced separately from the full NGC 4151 observation. Windows of 15 Å surrounding bright airglow lines in the total spectrum were then replaced by the corresponding intervals from the night-only spectrum. This eliminates most airglow features aside from geocoronal Lyα (which is greatly reduced in magnitude) and weak contributions from O II λ834 in first and second order, O I λ1304, and third order He I λ584.

[5] The Image Reduction and Analysis Facility (IRAF) is distributed by the National Optical Astronomy Observatories, which is operated by the Association of Universities for Research in Astronomy, Inc. (AURA), under cooperative agreement with the National Science Foundation.

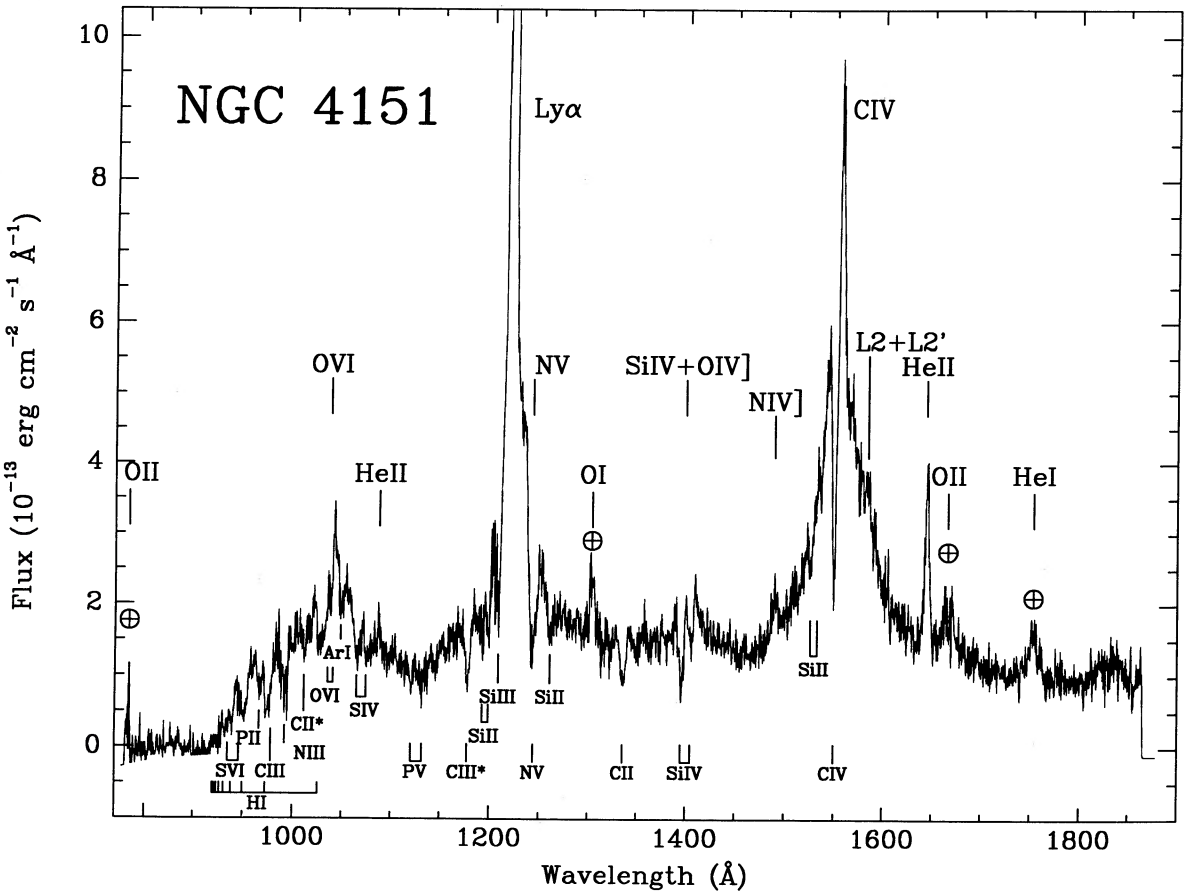

FIG. 1.—The flux-calibrated spectrum of NGC 4151 obtained with HUT is shown. Geocoronal Lyα has been subtracted. Identified emission and absorption features are marked above and below the data, respectively. Remaining airglow features in the spectrum are indicated with Earth symbols. The Lyα profile in NGC 4151 reaches a peak flux of 2.2×10^{-12} ergs cm^{-2} s^{-1} Å^{-1}, which is off scale in the figure.

The Lyα emission from NGC 4151 is blended with geocoronal Lyα. We developed an instrumental Lyα profile from observations of weak sources and blank fields obtained during the mission. This profile was scaled to the NGC 4151 observation using the short interval of airglow data obtained before the target was placed in the aperture and subtracted from the final spectrum. Figure 1 shows the final flux-calibrated HUT spectrum of NGC 4151. Identified emission and absorption features are marked in the figure. Many of the spectral features at wavelengths shortward of Lyα, such as O VI λλ1032, 1037 and He II λ1085 in emission, and C III λ977, N III λ991, O VI λλ1032, 1037, and the Lyman series in absorption, are seen for the first time in a low-redshift active galaxy.

3. DISCUSSION

Broad emission lines with FWHM ~ 8500 km s^{-1} from O VI λ1034, Lyα, Si IV + O IV] λ1400, and C IV λ1549 dominate the appearance of the HUT spectrum of NGC 4151. Numerous absorption lines punctuate the continuum and the wings of the broad lines, particularly below 1200 Å. All identified absorption features are blueshifted by 200–1300 km s^{-1} relative to the 984 km s^{-1} systemic velocity of NGC 4151. Longward of Lyα the spectrum is typical of that observed on many occasions with the *IUE*. The observed continuum flux level ($f_{1450} = 1.0 \times 10^{-13}$ ergs cm^{-2} s^{-1} Å^{-1}) and the observed flux of broad C IV λ1549 ($\sim 3.5 \times 10^{-11}$ ergs cm^{-2} s^{-1}) are slightly above the historical mean values (Clavel et al. 1991). Shortward of Lyα, however, the continuum shows a pronounced dip centered at ~ 1130 Å, and then turns over sharply below 1000 Å. The continuum is undetectable at 924 Å, well above the redshifted Lyman edge of NGC 4151 at 915 Å. This shape is not an instrumental calibration problem—other AGNs and hot stars observed by HUT have strong flux up to the Lyman limit of our own Galaxy (Davidsen et al. 1992).

3.1. *Emission Lines*

The broad emission lines have two distinct components—cores with FWHM of ~ 1500 km s^{-1}, and a much broader component with FWHM ~ 8500 km s^{-1}. The shape of the broad component is well described by a power law, $f_\lambda \sim (\lambda/\lambda_0)^{\pm\alpha}$ with $\alpha = 49.3$ for a FWHM of 8500 km s^{-1} ($\alpha = \ln 2/\ln[1 + \mathrm{FWHM}/2c]$, where c is the speed of light and FWHM is in km s^{-1}). This broad component dominates the flux of O VI λ1034, Lyα, N V λ1240, Si IV + O VI] λ1400, and C IV λ1549, but it is not detectable in the He II lines λ1640 and λ1085. These lines are dominated by the narrower core component which is also prominent in Lyα. The narrow core is not evident in O VI λ1034, perhaps being hidden by the strong O VI absorption.

To measure the emission line intensities we fit the NGC 4151 spectrum with a multicomponent model using a nonlinear χ^2 minimization technique. We use a power law continuum and allow for extinction according to the mean galactic curve of Seaton (1979), assuming it is valid to the Lyman edge as shown by *Voyager* observations (Longo et al. 1989; Snow, Allen, & Polidan 1990). Gaussian components are used for the narrower cores of the emission lines, while the broader components are fitted with the power-law form given above. Absorption lines are assumed to absorb both the continuum and the emission lines, and they have Gaussian profiles.

Table 1 gives emission-line fluxes measured from our spectrum of NGC 4151. The fluxes are corrected for the best-fit extinction of $E_{B-V} = 0.039$. For each line component we list the total flux, the heliocentric redshift cz, and the FWHM. We give the vacuum wavelengths of the lines for reference. The widths of the lines have not been corrected for the ~ 3 Å resolution of the instrument (750 km s^{-1} at 1200 Å). Error bars are computed from the covariance matrix of the fit for the appropriate $\Delta\chi^2$ as prescribed by Avni (1976) for the number of interesting parameters. For most lines these comprise five parameters: the continuum flux and slope, the line flux, mean wavelength, and FWHM. In cases where the tabulated error is zero, the parameter was fixed at the given value.

The best-fit, extinction-corrected power law for the continuum is $f_\lambda = 1.7 \times 10^{-13}(\lambda/1000\ \text{Å})^{-0.50}$ ergs cm^{-2} s^{-1} Å^{-1} with $E_{B-V} = 0.039$. For comparison, foreground galactic extinction along this line of sight is zero based on H I and galaxy counts (Burstein & Heiles 1978). Malkan & Sargent (1982) find $E_{B-V} = 0.06$ based on the strength of the 2175 Å absorption feature in the *IUE* spectrum, and a spectral index in f_λ of 0.8 for the optical through UV continuum.

The detection of He II λ1085 provides a diagnostic of the extinction toward the ~ 1500 km s^{-1} material in NGC 4151 since He II emission is likely to be due purely to recombination (Kwan & Krolik 1981; MacAlpine 1981; Krolik & Kallman 1988). This new diagnostic is significant since the reddening of the emission lines may differ from that of the continuum if dust is embedded in the clouds. Previous estimates of the extinction have ranged as high as $E_{B-V} = 0.24$ using the narrow-line region [S II] lines (Wampler 1971). Our measurement of the

TABLE 1

EMISSION LINES IN NGC 4151

Line	λ_{vac} (Å)	Flux (10^{-14} ergs cm^{-2} s^{-1})	$cz_\odot$ (km s^{-1})	FWHM (km s^{-1})
O VI	1033.83	2020 ± 140	1044 ± 520	9474 ± 1025
He II	1085.15	17 ± 10	677 ± 196	627 ± 438
Lyα	1215.67	1600 ± 120	1019 ± 65	1673 ± 127
Lyα	1215.67	3340 ± 160	2720 ± 712	9546 ± 639
N V	1240.15	3 ± 130	984 ± 0	8500 ± 0
Si IV	1396.76	940 ± 59	1721 ± 510	9944 ± 710
N IV]	1486.50	70 ± 28	807 ± 434	1878 ± 1013
C IV	1549.05	4400 ± 230	416 ± 224	7587 ± 486
C IV	1549.05	210 ± 78	1558 ± 182	875 ± 375
C IV (L2 + L2′)	1549.05	81 ± 37	6880 ± 695	2540 ± 609
He II	1640.50	180 ± 31	877 ± 88	1005 ± 223

NOTE.—All fluxes are corrected for extinction $E_{B-V} = 0.039$. Entries with error bars of zero are fixed at the tabulated value.

ratio of He II λ1640 to λ1085 implies a 2 σ upper limit of $E_{B-V} < 0.12$ for a density of 10^6 cm^{-3} and a temperature of 10,000 K. The upper limit is fairly insensitive to the assumed density and temperature.

The ratio of broad O VI λ1034 relative to broad C IV λ1549 is 0.46 ± 0.04, similar to that seen by Kinney et al. (1987) in intermediate-redshift quasars. The relative intensities of the broad components of C IV λ1549, Lyα, Si IV λ1400, and O VI λ1034 are all consistent with an ionization parameter log $U = -0.75$ (where U is the ratio of the density of ionizing photons to electrons) as suggested by the models of Ferland & Mushotzky (1982).

Although the profiles of C IV, Lyα, and O VI appear different from one another in a quick glance at Figure 1, the more direct comparison shown in Figure 2 reveals that they are similar. Here we have subtracted the best-fitting power-law continuum from the spectrum and superposed the line profiles in velocity space. All the broad-line profiles are heavily modified by overlying absorption and emission features, which are indicated. Allowing for these features, the profiles agree well. The apparent "dip" in the continuum at $\sim$1130 Å is simply the point at which the broad O VI λ1034 profile meets the blue wing of Lyα. The broad component of Lyα visible in our HUT spectrum was not previously visible with *IUE*. Clavel et al.

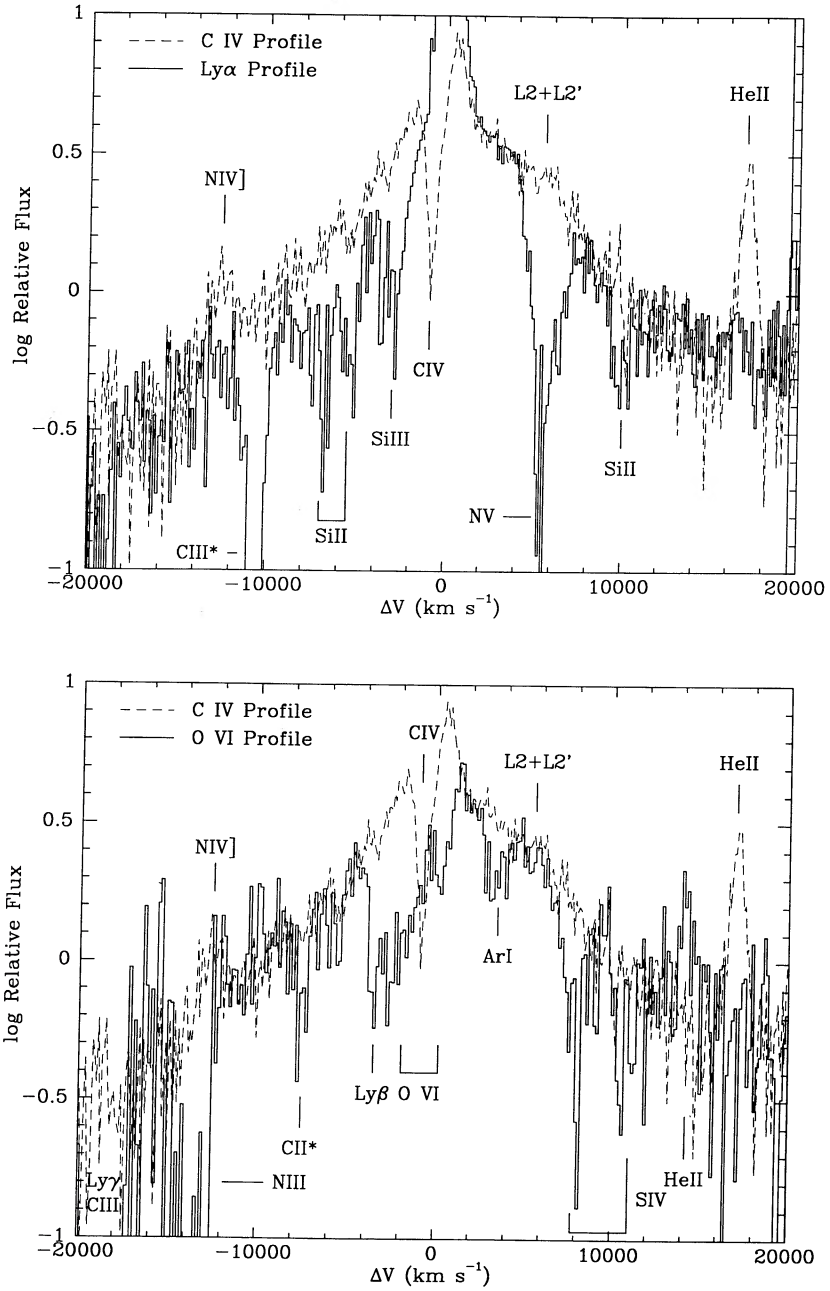

FIG. 2.—The broad emission-line profiles of Lyα (*a*) and O VI λ1034 (*b*) are compared to C IV λ1549. A power-law continuum has been subtracted as described in the text. Emission and absorption features lying in the wings of the broad lines are marked.

(1987) remark that there is no broad component of Lyα that corresponds to the broad profile of C IV in the high state of NGC 4151. The ease of detecting broad Lyα with HUT compared to *IUE* is entirely attributable to instrumental differences. The short-wavelength response of HUT permits us to measure the continuum shortward of the blue wing of Lyα, and the photon-counting detector allows reliable subtraction of geocoronal Lyα from the spectrum.

One of the C IV satellite lines first noticed by Ulrich et al. (1985) is also visible on the red side of the C IV profile. We see a broad feature centered at 1585 Å, the mean wavelength of the L2 λ1576 and L2′ λ1592 features. The fainter L1 line at 1518 Å is not apparent. The intensity of the red satellite line is comparable to the mean intensity of L2 + L2′ as given by Clavel et al. (1987).

3.2. *Absorption Lines*

Numerous absorption features are visible in the NGC 4151 spectrum, especially shortward of Lyα. Particularly prominent are the hydrogen Lyman series, C III λ1176, the O VI λλ1032, 1037 doublet, N III λ991, and C III λ977. All these strong features are significantly broader than the instrumental resolution of ~3 Å and have intrinsic widths of ~1000 km s^{-1}. The 200–1300 km s^{-1} blueshifts of the absorption lines place them nearly at their rest wavelengths in the observed frame, obscuring any features due to our own Galaxy. The intrinsic breadth of the features, their high equivalent widths, and their variability in previous studies with *IUE* (Bromage et al. 1985) all argue for intrinsic absorption in NGC 4151. Table 2 lists the observed properties of the strongest absorption lines in the HUT spectrum. We list all lines with equivalent widths greater than 1.4 Å (approximately our 5 σ detection threshold) and label the lines in Figure 1. Lines with uncertain identifications are enclosed by parentheses in Table 2.

TABLE 2

ABSORPTION LINES IN NGC 4151

Line	λ_{vac} (Å)	EW (Å)	$cz_{\odot}$ (km s^{-1})	FWHM (km s^{-1})
(S VI)	933.38	3.59 ± 1.22	260 ± 434	1643 ± 1026
(S VI)	944.52	2.20 ± 1.59	260 ± 0	1643 ± 0
Lyδ	949.74	3.73 ± 0.54	429 ± 181	1533 ± 0
(P II)	963.81	1.53 ± 0.34	647 ± 306	1646 ± 2159
Lyγ	972.54	3.13 ± 0.60	0 ± 154	1533 ± 0
C III	977.03	2.67 ± 0.50	−279 ± 188	1351 ± 160
N III	991.00	2.82 ± 0.76	424 ± 276	1607 ± 475
C II*	1010.13	1.99 ± 1.14	347 ± 665	1821 ± 1354
Lyβ	1025.72	3.84 ± 0.50	286 ± 148	1533 ± 89
O VI	1031.93	3.15 ± 0.57	−9 ± 217	1808 ± 369
O VI	1037.62	2.27 ± 0.50	81 ± 215	1475 ± 376
(Ar I)	1048.22	1.60 ± 1.20	137 ± 753	1653 ± 1611
(S IV)	1062.67	2.23 ± 1.40	714 ± 738	1841 ± 1340
(S IV)	1073.28	1.59 ± 1.59	564 ± 1177	1867 ± 2460
(P V)	1117.98	1.67 ± 1.30	676 ± 806	1663 ± 2409
(P V)	1128.01	2.64 ± 1.96	742 ± 875	1920 ± 1475
C III*	1175.70	2.59 ± 0.27	382 ± 86	1249 ± 148
Si II	1191.50	1.95 ± 0.37	75 ± 1260	1816 ± 810
Si II*	1195.50	1.40 ± 1.04	677 ± 194	883 ± 575
Si III	1206.50	2.01 ± 0.51	348 ± 409	1434 ± 649
N V	1240.15	6.54 ± 0.43	689 ± 294	2274 ± 177
Si II	1260.42	2.53 ± 0.36	67 ± 154	1326 ± 239
C II	1334.53	2.73 ± 0.43	487 ± 145	1337 ± 145
Si IV	1393.76	3.26 ± 0.34	568 ± 86	1229 ± 133
Si IV	1402.77	1.79 ± 0.53	327 ± 235	1229 ± 0
C IV	1549.05	3.66 ± 0.21	184 ± 41	976 ± 64

NOTE.—Absorption lines with uncertain identifications are enclosed in parentheses. Lines arising from excited metastable levels are indicated by an asterisk. Entries with error bars of zero are fixed at the tabulated value. Note that the EW error bars do not represent the statistical significance of a feature, but rather the uncertainty in measuring the EW simultaneously with the other fitted parameters. All listed features are significant at >5 σ.

The Doppler parameter of the absorbing material is constrained by our observations of the resolved Si IV λλ1393, 1402 doublet and the hydrogen Lyman lines. The Si IV doublet ratio of 1.82 ± 0.36 (90% confidence) favors only slight saturation in these lines. This gives a lower limit of $b > 190$ km s^{-1} at the 90% confidence level. Dopper parameters of ~200 km s^{-1} can also simultaneously explain the high equivalent widths in the higher order Lyman lines and the abrupt drop in the continuum level below 1000 Å. The continuum shape and a curve-of-growth analysis for the Lyman lines constrain the Doppler parameter to the range 150 km s^{-1} < b < 250 km s^{-1}. For b = 200 km s^{-1} and a neutral hydrogen column of 2.9 × 10^{19} cm^{-2}, the blended absorption from the converging Lyman series is sufficient to completely obscure the continuum below 924 Å. This is illustrated in Figure 3 where we compare the best-fit model including absorption by the Lyman lines to a model with no hydrogen absorption. Because all the Lyman lines fall on the flat portion of the curve of growth, however, the neutral hydrogen column is not well constrained. Columns in the range 17.8 < log N_{H^0} < 20.8 for 150 km s^{-1} < b < 250 km s^{-1} all give acceptable fits to the Lyman line equivalent widths and the short wavelength turnover of the spectrum.

Bromage et al. (1985) argue that absorption by the excited metastable level of C III at λ1176 and its strength relative to C IV λ1549 require this state to be collisionally populated in a high-density medium with $n_e > 10^{10}$ cm^{-3}. The equivalent widths measured from the HUT spectrum support this conclusion. Since strong absorption by the C III λ977 resonance line is also visible in the HUT spectrum, we can more fully determine the properties of the absorbing medium. To examine the populations in the C III ground state ^1S_L and the $^3P^o$ excited state, we follow Bromage et al. (1985) and consider radiative transitions from $^3P^o$ to ^1S_L, collisional excitation from $^3P^o$ to $^3P^e$, $^1P^o$, $^1D^e$, and ^1S_U, collisional de-excitation from $^3P^o$ to ^1S_L, and photoionization from $^3P^o$. This is balanced by recombination from C IV and collisional excitation of $^3P^o$ from the ground state:

$$n_{III^*}(A_{21} + n_e \Sigma q + R_I) = \alpha_2 n_e n_{IV} + n_e n_{III} q_{12} ,$$

where n_{III^*} = density in the $^3P^o$ level, n_{III} = density in the ground state ^1S_L, n_{IV} = density of C^{3+}, n_e = electron density, A_{21} = radiative transition probability from $^3P^o$ to ^1S_L, Σq = sum of the collisional rates from $^3P^o$ to $^3P^e$, $^1P^o$, $^1D^e$, and ^1S_L, R_I = photoionization rate from $^3P^o$, α_2 = effective recombination coefficient to $^3P^o$ (including di-electronic recombination), and q_{12} = collisional excitation rate from ^1S_L to $^3P^o$.

Solving for the relative population of $^3P^o$ to ^1S_L, we obtain

$$\frac{n_{III^*}}{n_{III}} = \left(\frac{\alpha_2}{\Sigma q}\frac{n_{IV}}{n_{III}} + \frac{q_{12}}{\Sigma q}\right) \Big/ \left(1 + \frac{A_{21}}{n_e \Sigma q} + \frac{R_I}{n_e \Sigma q}\right) .$$

To evaluate this numerically, we use collisional excitation rates from Dufton et al. (1981), transition probabilities from Nussbaumer & Storey (1979), and di-electronic recombination coefficients from Storey (1981). For the incident flux in the calculation of the photoionization rate, we assume a distance of 10^{17} cm from the source and extrapolate our best-fit power-law spectrum. Under these assumptions $R_I/A_{21} \sim 0.01$. Since $^1P^o$, $^1D^e$, $^3P^e$, and ^1S_U are all connected to lower levels by permitted radiative transitions, full collisional equilibrium is not achieved with the $^3P^o$ level unless the density is $\gtrsim 10^{16}$

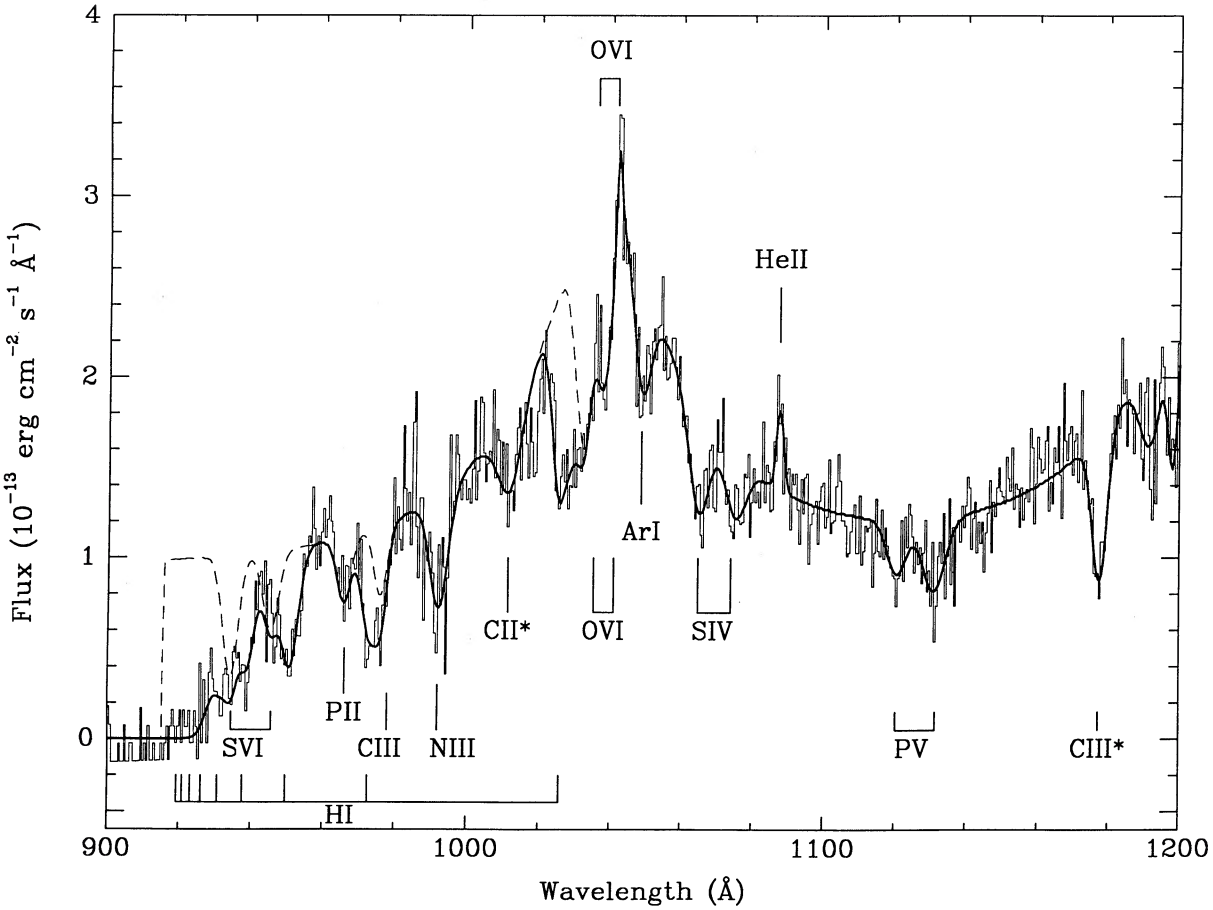

FIG. 3.—The far-UV spectrum of NGC 4151 in the 900–1200 Å wavelength range is shown to illustrate how blended absorption in the high-order lines of the Lyman series can effectively absorb the short-wavelength continuum. The data are shown as a histogram, and the heavy solid line shows the best-fitting power law as modified by extinction of $E_{B-V} = 0.039$, absorption by neutral hydrogen with $b = 200$ km s^{-1} and $N_H = 2.9 \times 10^{19}$ cm^{-2}, and additional Gaussian absorption lines with parameters as given in Table 2. The dashed line shows the model *without* the hydrogen absorption taken into account.

cm^{-3}. At lower densities the maximum ratio for n_{III*}/n_{III} is $n_{III*}/n_{III} = q_{12}/\Sigma q = 0.225$ at 50,000 K.

If we assume that n_{III*}, n_{III}, and n_{IV} coexist in a homogeneous region, then we can directly relate the ratios of inferred column densities to the space densities of these species. We note, however, that the different velocities measured for many of the absorption lines suggest some stratification in the absorbing region. Forcing the lines to all have the same redshift leads to significantly worse fits to the overall spectrum. From the equivalent widths of C III λ977 and C IV λ1549, we find a maximum ratio for the respective column densities of $N_{III}/N_{IV} = 1.82$ at the 90% confidence level. Substituting this for n_{IV}/n_{III} under the assumption of homogeneity, we evaluate our expression for n_{III*}/n_{III} over a range of densities and temperatures typical of the broad-line and narrow-line regions. The results are shown in Figure 4. Over the density range shown, n_{III*}/n_{III} reaches its maximum value for $T \simeq 50{,}000$ K. Dashed horizontal lines show the 90% confidence *lower* limits on the column-density ratio N_{III*}/N_{III} for various assumed values of the Doppler parameter. One can immediately see that Doppler parameters exceeding 400 km s^{-1} are ruled out. For Doppler parameters in the 150–200 km s^{-1} range preferred by our analysis of the Si IV doublet and the Lyman lines, one also finds that a minimum density $\sim 10^7$ cm^{-3} is necessary to achieve a ratio of n_{III*}/n_{III} compatible with the lower limit on the inferred ratio N_{III*}/N_{III}. For $b = 200$ km s^{-1}, the measured values of the equivalent widths suggest $n_e \gtrsim 10^{9.5}$ cm^{-3} for $T < 30{,}000$ K, temperatures more typical of the line emitting gas in AGNs.

Doppler parameters of $\sim$200 km s^{-1} are significantly greater than thermal velocities within the broad line clouds, but they are not high enough to explain the inferred intrinsic widths of the absorption lines. A consistent picture of the absorbing region requires many clumps of dense material with a velocity spread of $\sim$200 km s^{-1} within each clump, and relative velocities of $\sim$1000 km s^{-1} between clumps. The clumps must cover a substantial fraction of the continuum source and of the broad-line region along the line of sight. The blueshifts of the absorption lines, their large intrinsic widths, the wide range of ionization states, and the high inferred densities suggest that the absorbing material may be the disintegrating remnants of outflowing, radiatively accelerated broad-line clouds. Based on the similarity in line width between the absorption lines and the narrow core of Lyα, it is possible that the same material is responsible for both the absorption lines and the $\sim$1500 km s^{-1} cores of the broad emission lines. For a covering fraction f, the Lyα emission from clumps with densities n_e and an equivalent hydrogen column N_H is $L_{Ly\alpha} = 4\pi f \alpha_B n_e N_H r^2 hc/\lambda_\alpha$, where r is the radius of the emitting region. If we take $r \sim 10^{17}$ cm, just outside the broad-

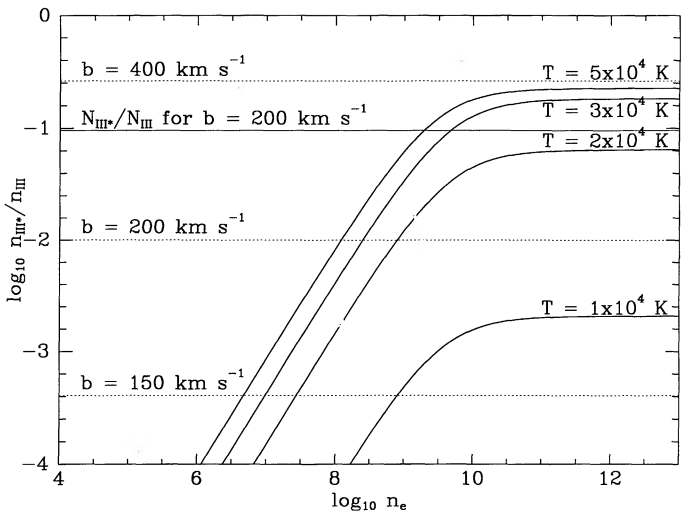

FIG. 4.—The heavy solid lines show the logarithm of the ratio of the space densities of the $^3P^o$ excited metastable level of C III to the ground state as a function of electron density at assumed gas temperatures of 1×10^4 K, 2×10^4 K, 3×10^4 K, and 5×10^4 K. The horizontal dashed lines are the 90% confidence lower limits on the *column* density ratio N_{III*}/N_{III} from our measured equivalent widths of C III λ977 and C III λ1176 for Doppler parameters $b = 150$, 200, and 400 km s^{-1}. The solid horizontal line is the inferred N_{III*}/N_{III} ratio for $b = 200$ km s^{-1}. The measured equivalent widths favor high gas densities and temperatures typical of broad-line cloud material in AGNs.

line region (Clavel et al. 1987; Maoz et al. 1991), we obtain $L_{Ly\alpha} = 5.32 \times 10^{41} f(n_e/10^{10}\ \mathrm{cm}^{-3})(N_H/10^{20}\ \mathrm{cm}^{-2})(r/10^{17}\ \mathrm{cm})^2$ ergs s^{-1}. For $f = 1$ this is comparable to the extinction-corrected luminosity in the narrow core of Lyα of 7.4×10^{41} ergs s^{-1} (for $H_0 = 50$ km s^{-1} Mpc^{-1}), but the correspondence may be fortuitous since the constraints on n_e, N_H, and the radius are all poor.

The column densities we infer are insufficient to explain the low-energy X-ray absorption in NGC 4151 (see also Bromage et al. 1985). For $b = 200$ km s^{-1}, we derive a column density for C^+, C^{+2}, and C^{+3} of 0.5×10^{15} cm^{-2} + 3.9×10^{15} cm^{-2} + 1.1×10^{15} cm^{-2} = 5.5×10^{15} cm^{-2}. Assuming this is the total column density in carbon and a cosmic abundance ratio yields a total equivalent hydrogen column of 1.7×10^{19} cm^{-3}. This value can be compared to the X-ray column of $\sim 1 \times 10^{22}$ cm^{-2} found by Holt et al. (1980). Significantly more UV-absorbing material may be present along the line of sight, however, if it has small Doppler parameters (< 50 km s^{-1}). We cannot rule out the presence of such material, whose detection will require future studies of the absorption line profiles at high resolution with the *Hubble Space Telescope*.

4. SUMMARY

Far-ultraviolet observations of the Seyfert galaxy NGC 4151 with the Hopkins Ultraviolet Telescope reveal a number of spectral features in the 912–1150 Å range that are seen for the first time in a low-redshift active galaxy, including emission from O VI $\lambda\lambda$1032, 1037 and He II λ1085, and absorption by C III λ977, N III λ991, O VI $\lambda\lambda$1032, 1037, and the hydrogen Lyman series. The broad emission lines all have similar profiles—broad cores of FWHM $\sim$1500 km s^{-1} are accompanied by a much broader component of FWHM $\sim$8500 km s^{-1}. The relative line intensities are consistent with previously calculated photoionization models. Numerous broad absorption lines of FWHM $\sim$1000 km s^{-1} blueshifted by 200 to 1300 km s^{-1} relative to the systemic velocity of NGC 4151 modify the appearance of the spectrum, particularly shortward of Lyα. The continuum turns over sharply below 1000 Å and disappears by 924 Å, well above the redshifted Lyman edge. Absorption by the converging high-order Lyman lines in material with a Doppler parameter $b = 200$ km s^{-1} can explain the turnover of the continuum. Such larger Doppler parameters are also consistent with the ratio of equivalent widths observed in the Si IV $\lambda\lambda$1393, 1402 doublet and the C III lines at λ977 and λ1176. The inferred column densities of absorbing material producing the C III absorption lines λ977 and λ1176 require a density in excess of $10^{9.5}$ cm^{-3}. The blueshifted absorption, the inferred high density of the absorbing material, and the similarity of the widths to the cores of the broad lines suggest that the absorbing medium is outflowing gas from the broad-line region.

We are grateful to the many members of the HUT team at JHU and APL who contributed to the flawless performance of HUT. Special thanks go to the Spacelab Operations Support Group at Marshall Space Flight Center whose superb efforts to overcome the many problems during the flight of Astro-1 are in large part responsible for the high quality of the resulting scientific data. This work was supported by NASA contract NAS 5-27000 to The Johns Hopkins University.

REFERENCES

Anderson, K. S. 1974, ApJ, 189, 195
Antonucci, R. R. J., & Cohen, E. D. 1983, ApJ, 271, 564
Avni, Y. 1976, ApJ, 210, 642
Bromage, G. E., et al. 1985, MNRAS, 215, 1
Burstein, D., & Heiles, C. 1978, ApJ, 225, 40
Clavel, J., et al. 1992, ApJ, 393, in press
———. 1987, ApJ, 321, 251
Davidsen, A. F., et al. 1992, ApJ, 392, 264
Dufton, P. L., Berrington, K. A., Burke, P. G., & Kingston, A. E. 1978, A&A, 62, 111
Ferland, G. J., & Mushotzky, R. F. 1982, ApJ, 262, 564
Holt, S. A., Mushotzky, R. F., Becker, R. H., Boldt, E. A., Serlemitsos, P. J., Szymkowiac, A. E., & White, N. E. 1980, ApJ, 241, L13
Kinney, A. L., Huggins, P. J., Glassgold, A. E., & Bregman, J. N. 1987, ApJ, 314, 145
Krolik, J., & Kallman, T. 1988, ApJ, 324, 714
Kwan, J., & Krolik, J. H. 1981, ApJ, 250, 478
Longo, R., Stalio, R., Polidan, R. S., & Rossi, L. 1989, ApJ, 339, 474
MacAlpine, G. M. 1981, ApJ, 251, 465
Malkan, M. A., & Sargent, W. L. W. 1982, ApJ, 254, 22
Maoz, D., Netzer, H., Mazeh, T., Beck, S., Almoznino, E., Leibowitz, E., Brosch, N., Mendelson, H., & Laor, A. 1991, ApJ, 367, 493
Nussbaumer, H., & Story, P. J. 1978, A&A, 64, 139
Osterbrock, D. E., & Koski, A. T. 1976, MNRAS, 176, 61P
Penston, M. V., et al. 1981, MNRAS, 196, 857
Seaton, M. J. 1979, MNRAS, 187, 75P
Seyfert, K. 1943, ApJ, 97, 28
Snow, T. P., Allen, M. M., & Polidan, R. S. 1990, ApJ, 359, L23
Storey, P. J. 1981, MNRAS, 195, 27P
Ulrich, M. H., et al. 1984, MNRAS, 206, 221
———. 1985, Nature, 313, 745
Wampler, E. J. 1971, ApJ, 164, 1